

A Solid-Shell Element with Enhanced Assumed Strains for Higher Order Shear Deformations in Laminates

Nguyen Dang Quy, A. Matzenmiller

In structural analysis the three-dimensional standard 8-node brick element has become one of the most favourable elements, especially due to its numerical efficiency, its versatility and its wide range of applicability to many types of mechanical problems. However, low-order elements, based on the irreducible displacement model, suffer from different kind of locking effects. For instance, shear locking occurs in the finite element analysis of thin plates or shells under flexural deformations. In this case pure bending modes can not be represented by the standard linear element due to the parasitic shear deformation. By using higher order elements, these locking phenomena are reduced, but the computational effort becomes larger. To overcome this deficiency, numerous investigations have been undertaken for finding a high accurate, low-order element without increasing the computational cost significantly.

Based on previous research, our approach aims towards the analysis of laminated structures with solid-shell elements, combined with the higher order shear deformation theory to improve the transverse shear behaviour, necessary for stress based failure criteria in the analysis of inter-laminar fracture in multi-layer shells. As a side effect shear-locking is alleviated by incorporating the higher order transverse shear interpolation instead of using assumed natural strain formulations. The solid-shell element is used for the analysis of delamination in layered composite shells, where the onset of fracture in mode II and III critically depends on the transverse shear stress distribution in the cross section of the shell.

1 Introduction

Multi-layer composite shell structures are used for a wide range of applications in engineering design, e.g. for bridges and roofs in civil engineering, for car bodies in the automotive industry, or for light weight components in aero space structures. Several shell elements, based on a reference surface, have been investigated and developed in the past. Low-order solid-shell elements are now in the focus for the analysis of general shell structures and have drawn interest for a number of years. However, there is still a continuing need for more accurate and efficient solid-shell elements, especially if they are used for the load carrying analysis of layered composite structures, where a reliable resolution of the transverse shear strain and stress is required. If the number of nodes and elements through the thickness of the layered composite shell shall be kept low, it may be resorted to higher order shear deformation theories (HOSDT), where the transverse shear strain and stress distribution is improved as outlined for example in Liu and Reddy (1985), Nguyen et al. (2004), Rastgaar and Aagaah (2003), Reddy (2004) and Reddy and Lee (2004). In this paper an elegant way of incorporating parabolic enhanced transverse shear and normal strain interpolations into low order shell elements is discussed, which show poor transverse strain and stress distributions through the thickness in the case of pure and linear bending.

Recent approaches to improve the element performance for shell analysis can be classified into two categories, namely the assumed stress and the enhanced assumed strain method (EAS). The first one is based on the HELLINGER-REISSNER functional with displacement and stresses as independent field variables (Marotti, 2002) - and boils down to a pure displacement method by pre-elimination of the stress parameters. The enhanced assumed strain method (EAS) adopts the three-field functional of the HU-WASHIZU type with displacements, strains, and stresses as independent primary variables and may be reduced to a FE-displacement scheme by stipulating orthogonality between the enhanced strain and stress fields and static condensation of the parameters for the incompatible strain field – see Simo and Rifai (1990). From a computational point of view the assumed stress approach is more efficient than the enhanced assumed strain method. However, the implementation of a general nonlinear constitutive model is more difficult in the first case, whereas the second approach makes direct use of a strain energy function.

With regard to computational shell analysis one may distinguish between shell formulations, describing the deformation of a reference surface in a thin-walled structure or solid-shell formulations, modelling the motion of the top and bottom surface of the shell – see Krätzig and Jun (2002) and Schweizerhof (2001). In the recent past such solid-shell elements have been developed, which show similar accuracy as degenerated elements but comprise complete three-dimensional constitutive relations between stresses and strains without any further modification such as degeneration of the constitutive tensor. But the second main assumption of the degenerated shell concept that the normal to the element mid-surface remains straight but not necessarily orthogonal during the deformation process is inherent in the solid-shell approach. In the sense of higher order shear deformation theories (HOSDT) the continuum based 3D-shell element is endowed with an improved transverse shear stress interpolation for the simulation of the delamination in layered, thin-walled composite structures. The standard 8-node brick element with tri-linear shape functions forms the basis of the present finite shell element together with the EAS method as outlined in Fiolka and Matzenmiller (2007). The enhanced assumed strain method (EAS) is applied to the transverse shear strain field to improve the transverse shear stress distribution necessary for stress based failure criteria and to alleviate shear locking as a side effect. It is assumed that the stress field and the interpolation of the incompatible strains are orthogonal, which results in the elimination of the stress field parameters from the discretized variational equations. In comparison to some other proposals the approach presented here allows the use of a lower number of strain variables, which favours the computational efficiency. When dealing with geometrical non-linearity, the original setting is still kept for an additive enhancement of the displacement-based convective Green–Lagrange strains in a way successfully employed in Ramm and Andelfinger (1993), after that in Klinkel and Wagner (1997) and recently consolidated by Vu-Quoc and Tan (2003).

2 Kinematical Formulation of Solid-Shell Element

In this section a solid-shell concept is described that circumvents the well-known problems with the rotational degrees of freedom for degenerated shell elements. The following figure shows the reference and current configuration and the kinematics of the solid-shell element in curvilinear coordinates.

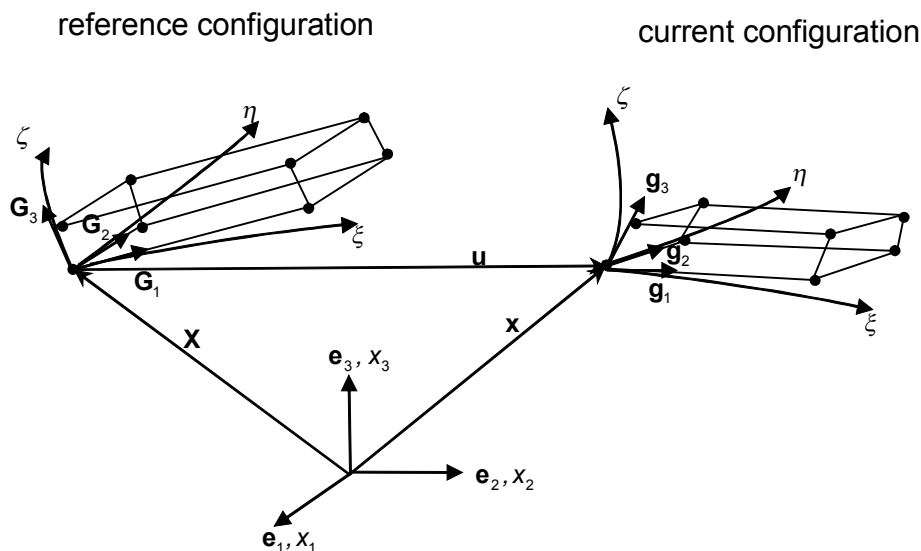


Figure 1. Convected base vectors and curvilinear coordinates of linear solid-shell element

Each point on the upper or lower surface of the three-dimensional shell-like continuum in its initial configuration is endowed with its position vector \mathbf{X}_u or \mathbf{X}_l respectively.

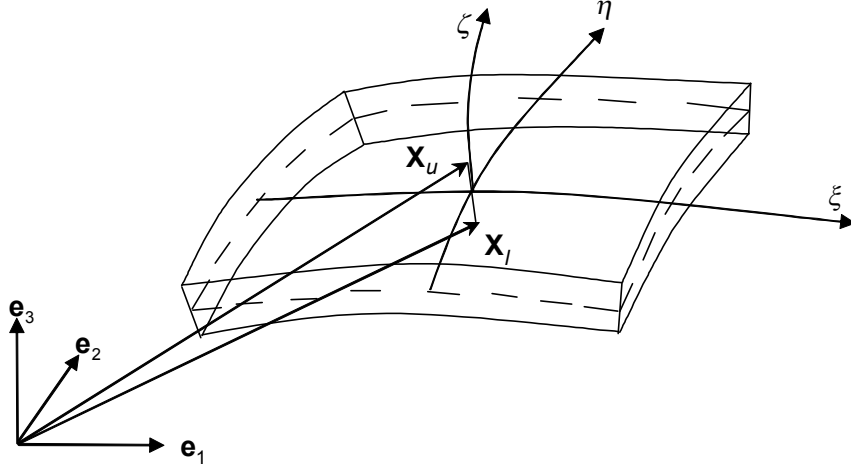


Figure 2. Geometry of shell with position vectors of points on upper and lower surface

In the solid-shell concept the variables ξ and η are the local convective coordinates in two independent in-plane directions and ζ is the local convective coordinate in the thickness direction. The vector \mathbf{X} and the displacement field \mathbf{u} of each point of the shell-like continuum are described by the position vector \mathbf{X}_u and its displacement vector \mathbf{u}_u of the corresponding points on the upper shell surface and on the lower one by \mathbf{X}_l and \mathbf{u}_l .

$$\mathbf{X}(\xi, \eta, \zeta) = \frac{1}{2}[(1 + \zeta)\mathbf{X}_u(\xi, \eta) + (1 - \zeta)\mathbf{X}_l(\xi, \eta)] \quad (1)$$

Rewriting the equation for the initial geometry as follows:

$$\mathbf{X}(\xi, \eta, \zeta) = \frac{1}{2}[\mathbf{X}_u(\xi, \eta) + \mathbf{X}_l(\xi, \eta)] + \frac{1}{2}\zeta[\mathbf{X}_u(\xi, \eta) - \mathbf{X}_l(\xi, \eta)] \quad (2)$$

and similarly for the current configuration:

$$\mathbf{x}(\xi, \eta, \zeta) = \frac{1}{2}[\mathbf{x}_u(\xi, \eta) + \mathbf{x}_l(\xi, \eta)] + \frac{1}{2}\zeta[\mathbf{x}_u(\xi, \eta) - \mathbf{x}_l(\xi, \eta)] \quad (3)$$

The relation $\mathbf{x} = \mathbf{X} + \mathbf{u}$ leads to the description of the geometry in the actual state which is essential for the evaluation of the deformation gradient. The notation ξ , η and ζ for the local coordinates is abbreviated for the purpose of index notation and summation convention into ξ^i with $\xi^1 = \xi$, $\xi^2 = \eta$ and $\xi^3 = \zeta$ in the next equations.

The covariant base vectors are obtained from the position vectors of the reference configuration \mathbf{X} and the current one \mathbf{x} by their partial derivatives with respect to the convective coordinates:

$$\mathbf{G}_i = \frac{\partial \mathbf{X}}{\partial \xi^i} \quad \text{and} \quad \mathbf{g}_i = \frac{\partial \mathbf{x}}{\partial \xi^i} \quad (4)$$

The contravariant base vectors \mathbf{G}^i and \mathbf{g}^i are defined as follows:

$$\mathbf{G}_i \mathbf{G}^j = \delta_j^i \quad \text{and} \quad \mathbf{g}_i \mathbf{g}^j = \delta_j^i \quad (5)$$

Then the deformation gradient is given by the sum of dyadic products:

$$\mathbf{F} = \mathbf{g}_i \otimes \mathbf{G}^i \quad (6)$$

Therefore, the Green–Lagrange strain tensor is computed by the formula:

$$\mathbf{E}^u = E_{ij}^u \mathbf{G}^i \otimes \mathbf{G}^j \quad \text{with} \quad E_{ij}^u = \frac{1}{2}(\mathbf{g}_{ij} - \mathbf{G}_{ij}), \quad \text{where } (i, j = 1, 2, 3) \quad (7)$$

and the metric coefficients of the reference and current configuration:

$$G_{ij} = \mathbf{G}_i \mathbf{G}_j \quad \text{and} \quad g_{ij} = \mathbf{g}_i \mathbf{g}_j \quad (8)$$

3 Enhanced Assumed Strain Method (EAS Method)

The enhanced assumed strain method (EAS) in Simo and Rifai (1990) evolved from Wilson et al. (1973) and Taylor et al. (1976) for the purpose of improving the performance of the irreducible displacement model by adding an additional term $\tilde{\mathbf{E}}$ to the compatible strain field $\mathbf{E}^u(\mathbf{u})$.

$$\mathbf{E} = \mathbf{E}^u(\mathbf{u}) + \tilde{\mathbf{E}}(\alpha) \quad \text{and} \quad \delta \mathbf{E} = \delta \mathbf{E}^u(\mathbf{u}) + \delta \tilde{\mathbf{E}}(\alpha) \quad (9)$$

The tensor $\tilde{\mathbf{E}}(\alpha)$ denotes the enhanced part of the strain, depending on the parameters α_i , assembled in the vector α . The parameters can be eliminated on the element level and, thus, the formulation preserves the original character of the displacement based method.

The EAS method, based on a three-field variational principle of HU-WASHIZU, is defined by the functional:

$$\Pi(\mathbf{u}, \tilde{\mathbf{E}}, \sigma) = \int_{\Omega} W(\mathbf{x}, \mathbf{E}^u + \tilde{\mathbf{E}}) d\Omega - \int_{\Omega} \tilde{\mathbf{E}}^T \sigma d\bar{\mathbf{t}} - \int_{\Omega} \mathbf{u}^T \bar{\mathbf{b}} d\Omega - \int_{\Gamma_{\sigma}} \mathbf{u}^T \bar{\mathbf{t}} d\Gamma \quad (10)$$

where W denotes the stored energy function, $\bar{\mathbf{b}}$ the body forces throughout the domain Ω of the structure and $\bar{\mathbf{t}}$ the surface tractions on the force boundary Γ_{σ} of the body. Setting the first variation $\delta \Pi$ equal to zero, eq. (10) leads to the three variational equations:

$$\int_{\Omega} \delta \tilde{\mathbf{E}}^T \left(\frac{\partial}{\partial \tilde{\mathbf{E}}} W(\mathbf{x}, \mathbf{E}^u + \tilde{\mathbf{E}}) - \sigma \right) d\Omega = 0 \quad (11)$$

$$\int_{\Omega} \delta \sigma^T \tilde{\mathbf{E}} d\Omega = 0 \quad (12)$$

$$\int_{\Omega} \delta \mathbf{E}^{uT} \sigma d\Omega - \int_{\Omega} \delta \mathbf{u}^T \bar{\mathbf{b}} d\Omega - \int_{\Gamma_{\sigma}} \delta \mathbf{u}^T \bar{\mathbf{t}} d\Gamma = 0 \quad (13)$$

In the context of the finite element approximation the coordinates of the position vector \mathbf{X} and the ones of the displacement field \mathbf{u} are interpolated by using the standard isoparametric shape functions. The enhanced strain field is computed by:

$$\tilde{\mathbf{E}} = \mathbf{G}(\xi, \eta, \zeta) \alpha^e, \quad (14)$$

where $\mathbf{G}(\xi, \eta, \zeta)$ is the interpolation matrix, which is chosen as a function of the convective coordinates and can be extend in different modifications of the element and α^e is the vector with the free parameters for the enhanced strain distribution of the element. Since only C^1 -continuity is required at the inter-element boundaries for the enhanced strain field, the resulting system of algebraic equations may be solved for the parameters α^e on for each element individually by static condensation for quasi-static problems as it is typical for hybrid FE-methods. Then, the total strain field is given as:

$$\mathbf{E} \cong \mathbf{B}(\xi, \eta, \zeta) \mathbf{d}^e + \mathbf{G}(\xi, \eta, \zeta) \alpha^e \quad (15)$$

with \mathbf{B} as the discrete, linearized, kinematical operator of the finite element and \mathbf{d}^e as the vector of element nodal displacements. In eq. (15) the enhanced strain interpolation and the compatible part of the strains must be independent. In addition, the columns of the matrix $\mathbf{G}(\xi, \eta, \zeta)$ are assumed to be linearly independent. In important basic conditions is necessary to ensure the stability of the enhanced strain approximation, requiring the enhanced strain field to be orthogonal to the stress field:

$$\int_{\Omega} \tilde{\mathbf{E}}^T \delta \boldsymbol{\sigma} \, d\Omega = 0 \quad (16)$$

The treatment of the virtual stress field in the discretization process is not obvious in order to satisfy the orthogonality condition. If the distribution of virtual stresses is assumed constant throughout the element, then eq. (16) implies that the matrix $\mathbf{G}(\xi, \eta, \zeta)$ must have the property

$$\int_{\Omega} \mathbf{G}(\xi, \eta, \zeta) \, d\Omega = \mathbf{0} \quad (17)$$

which is only a sufficient condition to satisfy consistency. However, eq. (17) is overly restrictive for the incorporation of the HOSDT into the tri-linear brick element by means of the EAS-method, which rather relies on eq. (16).

4 Transverse Shear Strain Interpolation

Irreducible displacement models for linear finite LAGRANGE elements exhibit undesirable behaviour - called locking - under modes of pure bending or incompressibility. Locking occurs when the element fails to present a certain mode of deformation without parasitic strains and stresses. Transverse shear locking appears in low order thin plate or shell elements under pure bending moments in the absence of any transverse shear forces. It occurs only in elements, which take into account transverse shear deformations and is provoked by the parasitic transverse shear strains altering the pure bending deformation. The disproportional large stiffening depends on the aspect ratio of the elements (ratio of length to thickness) and becomes more pronounced as this proportion augments. In order to alleviate locking effects, many formulations, which include strains and stresses as additional primary fields have been proposed. In the continuum based 3D-shell element, previous modifications have used assumed natural strain (ANS) –see Bathe and Dvorkin (1986) or Stander et al. (1989) - or enhanced assumed strain (EAS) formulations, applied to the transverse shear strain field for the alleviation of the shear-locking phenomenon, see Klinkel et al. (1998, 1999), Klinkel and Wagner (1997), Vu-Quoc and Tan (2003), Ramm and Andelfinger (1993) and Fontes Valente et al. (2002), (2005) and (2006).

The interpolation of the incompatible strain components in eq. (14) is constructed by means of monomials of the curvilinear coordinates ξ , η and ζ of the shell. The VOIGT vector notation of the strains tensors

$$\mathbf{E}^u(\mathbf{u}) = (E_{11}^u, E_{22}^u, E_{33}^u, E_{12}^u, E_{13}^u, E_{23}^u) \quad \text{and} \quad \tilde{\mathbf{E}}(\mathbf{u}) = (\tilde{E}_{11}, \tilde{E}_{22}, \tilde{E}_{33}, \tilde{E}_{12}, \tilde{E}_{13}, \tilde{E}_{23}), \quad (18)$$

is used for the representation of the transverse shear strain enhancement with the interpolation matrix $\mathbf{G}(\xi, \eta, \zeta)$ as for constant JACOBIAN elements – see Taylor et al. (1976):

$$\mathbf{G}(\xi, \eta, \zeta) = \frac{\det \mathbf{J}_0}{\det \mathbf{J}} \mathbf{T}_0 \mathbf{M}(\xi, \eta, \zeta) \quad (19)$$

Here, \mathbf{J}_0 and \mathbf{J} denote the JACOBI matrices at the centre of the element and at the integration points for the GAUSS quadrature respectively. $\mathbf{M}(\xi, \eta, \zeta)$ is the interpolation matrix for the enhanced strain part in the EAS method and is specified below. \mathbf{T}_0 denotes the transformation matrix (Klinkel et al., 1999, Schweizerhof, 2001, Fiolka and Matzenmiller, 2007) of the strain tensor from the local coordinate chart at the element centre $\xi = \eta = \zeta = 0$ with the base vectors $\mathbf{G}_0^j := \mathbf{G}^j(\xi = \eta = \zeta = 0)$ in the cotangent space to the local convective coordinate system \mathbf{G}^j at the sampling points for the GAUSS integration of the element – see figure 1 with covariant base vectors \mathbf{G}_i of the tangent space. The elements T_{0ij} , denoted by

$$T_{0ij} := t_i^j := \mathbf{G}_i \cdot \mathbf{G}_0^j = \mathbf{G}_0^j \cdot \mathbf{G}_i \quad (20)$$

of the transformation matrix \mathbf{T}_0 are given as:

$$\mathbf{T}_0 = \begin{bmatrix} \begin{pmatrix} t_1^1 \end{pmatrix}^2 & \begin{pmatrix} t_1^2 \end{pmatrix}^2 & \begin{pmatrix} t_1^3 \end{pmatrix}^2 & t_1^1 t_1^2 & t_1^1 t_1^3 & t_1^2 t_1^3 \\ \begin{pmatrix} t_2^1 \end{pmatrix}^2 & \begin{pmatrix} t_2^2 \end{pmatrix}^2 & \begin{pmatrix} t_2^3 \end{pmatrix}^2 & t_2^1 t_2^2 & t_2^1 t_2^3 & t_2^2 t_2^3 \\ \begin{pmatrix} t_3^1 \end{pmatrix}^2 & \begin{pmatrix} t_3^2 \end{pmatrix}^2 & \begin{pmatrix} t_3^3 \end{pmatrix}^2 & t_3^1 t_3^2 & t_3^1 t_3^3 & t_3^2 t_3^3 \\ 2t_1^1 t_2^1 & 2t_1^2 t_2^2 & 2t_1^3 t_2^3 & t_1^1 t_2^2 + t_1^2 t_2^1 & t_1^1 t_2^3 + t_1^3 t_2^1 & t_1^2 t_2^3 + t_1^3 t_2^2 \\ 2t_1^1 t_3^1 & 2t_1^2 t_3^2 & 2t_1^3 t_3^3 & t_1^1 t_3^2 + t_1^2 t_3^1 & t_1^1 t_3^3 + t_1^3 t_3^1 & t_1^2 t_3^3 + t_1^3 t_3^2 \\ 2t_2^1 t_3^1 & 2t_2^2 t_3^2 & 2t_2^3 t_3^3 & t_2^1 t_3^2 + t_2^2 t_3^1 & t_2^1 t_3^3 + t_2^3 t_3^1 & t_2^2 t_3^3 + t_2^3 t_3^2 \end{bmatrix} \quad (21)$$

Based on the theoretical foundations of the high-order shear deformation theories, the main focus of this approach is put on the interpolation matrix $\mathbf{M} = \hat{\mathbf{M}}(\xi, \eta, \zeta)$. The transverse shear components of the strain field will be enhanced by incompatible parts in order to avoid shear locking and to allow parabolic shear strain fields as necessary for the deformation of plates and shells under transverse loading. In order to account for the higher order shear deformation theory, the interpolation matrix \mathbf{M} is defined for the enhanced transverse shear strains, as follows for the 8-node quadrilateral element Q8S12:

$$\mathbf{M} = \hat{\mathbf{M}}(\xi, \eta, \zeta) \quad (22)$$

$$= \begin{bmatrix} 0 & 0 & 0 & 0 & 0 & 0 & 0 & 0 & 0 & 0 & 0 & 0 & 0 \\ 0 & 0 & 0 & 0 & 0 & 0 & 0 & 0 & 0 & 0 & 0 & 0 & 0 \\ 0 & 0 & 0 & 0 & 0 & 0 & 0 & 0 & 0 & 0 & 0 & 0 & 0 \\ 0 & 0 & 0 & 0 & 0 & 0 & 0 & 0 & 0 & 0 & 0 & 0 & 0 \\ \xi & 0 & \xi\eta & 0 & \frac{1}{5} - \zeta^2 & 0 & \xi \left(\frac{1}{5} - \zeta^2 \right) & \eta \left(\frac{1}{5} - \zeta^2 \right) & 0 & 0 & \xi\eta \left(\frac{1}{5} - \zeta^2 \right) & 0 & 0 \\ 0 & \eta & 0 & \xi\eta & 0 & \frac{1}{5} - \zeta^2 & 0 & 0 & \xi \left(\frac{1}{5} - \zeta^2 \right) & \eta \left(\frac{1}{5} - \zeta^2 \right) & 0 & \xi\eta \left(\frac{1}{5} - \zeta^2 \right) & 0 \end{bmatrix}$$

Note, due to the parabolic strain interpolation in thickness direction \mathbf{G}_3 the integration rule must be changed to 2x2x3 GAUSS quadrature for the formation of the element stiffness matrix and the element force vector. It is easy to show that the term $\left(\frac{1}{5} - \zeta^2 \right)$ satisfies the orthogonality condition in eq. (16) for the well-known parabolic transverse shear stress distribution of engineering mechanics for beams under shear forces.

The interpolation matrix $\hat{\mathbf{M}}(\xi, \eta, \zeta)$ can be simplified and reduced to a constant and to linear monomials of the local coordinates for the enhanced transverse shear part for a computationally more efficient solid-shell element – see eq. (23a, b). The resulting elements are denoted as Q8S4 and Q8S8. They still allow a 2x2x2 GAUSS integration scheme for the element stiffness computation:

$$\mathbf{M} = \hat{\mathbf{M}}(\xi, \eta, \zeta) = \begin{bmatrix} 0 & 0 & 0 & 0 \\ 0 & 0 & 0 & 0 \\ 0 & 0 & 0 & 0 \\ 0 & 0 & 0 & 0 \\ \xi & 0 & \xi\eta & 0 \\ 0 & \eta & 0 & \xi\eta \end{bmatrix} \quad \text{and} \quad \mathbf{M} = \hat{\mathbf{M}}(\xi, \eta, \zeta) = \begin{bmatrix} 0 & 0 & 0 & 0 & 0 & 0 & 0 & 0 \\ 0 & 0 & 0 & 0 & 0 & 0 & 0 & 0 \\ 0 & 0 & 0 & 0 & 0 & 0 & 0 & 0 \\ 0 & 0 & 0 & 0 & 0 & 0 & 0 & 0 \\ \xi & \zeta & 0 & 0 & \xi\eta & \xi\zeta & 0 & 0 \\ 0 & 0 & \eta & \zeta & 0 & 0 & \xi\eta & \eta\zeta \end{bmatrix} \quad (23)$$

The extension of the transverse shear strain interpolation in element Q8S8 pays off, when the solution for the strain distribution provokes the linear part of the polynomials.

5 Finite Element Analysis of Thick Cantilever Beam ($L/h = 5$)

Typically a clamped thick beam is studied first for the numerical investigation of the element behaviour in order to verify the implementation and to validate the performance, the efficiency and the accuracy of the three transverse shear improved models as given in the eqs. (22), (23a) and (23b) above. The clamped, thick beam,

subjected to a concentrated loading P at the tip, is considered as a benchmark problem, where shear deformations are pronounced. The performance of the transverse shear improved element in this approach is compared to successful, standard, linear shell and solid-shell elements with enhancements according to the EAS and ANS method, published previously. The beam is divided into 10 three-dimensional linear solid-shell elements along the length for the finite element approximation – see figure 3. In order to improve the resolution for the transverse shear strain and stress distribution a finite element mesh with 16 layers of 8-node LAGRANGE bricks through the thickness is analysed under the assumptions of the small displacement theory. The results for the deflection and the shear strain and stress distributions are compared to the ones of a standard, simple discretization with only one element through the thickness but the same number of bricks along the length.

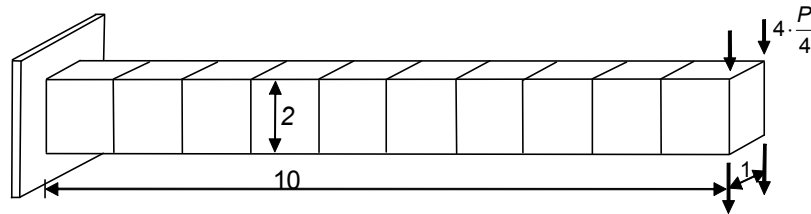


Figure 3. Geometry and FE-mesh of thick cantilever beam

In the figure above $b = 1$ cm is defined as the width, $L = 10$ cm as the length, and $h = 2$ cm as the thickness of the beam. The standard 8-node brick element Q8 with and without modified distributions of the transverse shear and normal thickness strains is used in the analysis of the beam. The performance of the different elements is compared in the diagrams below.

Since the transverse shear deformations contribute only little to the deflection of even a fairly thick beam of isotropic material, an anisotropic elasticity model with low transverse shear stiffness for the beam is chosen in order to increase the contribution of the transverse shear deformations as it is typically encountered in unidirectionally reinforced laminates of polymeric matrices with large shear compliance moduli and fibres of high stiffness. Thus, two numerical examples with an isotropic and a transverse isotropic, linear elastic constitutive model are considered. For the beam with the isotropic elastic material assumption YOUNG's modulus is $E = 100\,000$ N/mm², POISSON's ratio is taken as $\nu = 0.4$ and a point load of $P = 4\,000$ N is applied at the tip of the cantilever.

For the beam with the transverse isotropic model the elasticity parameters of the material are chosen as $E_1 = 3.11 \cdot 10^6$ N/cm², $E_2 = E_3 = 0.76 \cdot 10^6$ N/cm², $G_{12} = G_{13} = 0.29 \cdot 10^6$ N/cm², $G_{23} = 0.26 \cdot 10^6$ N/cm², $\nu_{12} = 0.303$ and the privileged axis in the direction of the centre line. The concentrated loading at the tip of the anisotropic beam is reduced to $P = 40$ N.

The deflection w_{\max} at the tip may be computed for the cantilever with I as the moment of inertia and A as the area of the cross section from classical engineering mechanics by means of the TIMOSHENKO theory for beams with flexure and transverse shear deformations:

$$w_{\max} = \frac{PL^3}{3EI} + \frac{PLh^2}{10GA} \quad (24)$$

It is equal to 0.2067 cm in the case of the isotropic material and equal to 0.659 cm in the one for the transversely isotropic constitutive assumption.

The results of a geometrical linear analysis for the displacement field in the transverse direction (ζ -direction) of the beam are plotted in Figures 4, 5, 6, 7, and 8 for various cases of elasticity models over the length of the cantilever for both thickness discretizations by means of the three different elements with strain interpolations as proposed above. They are compared to some well accepted solid-shell elements with assumed natural strains (ANS) – see Bathe and Dvorkin (1986) - and enhanced assumed natural strains (EAS). The specific element types are abbreviated by the following notation - see Klinkel et al. (1999) and appendix:

- Q8: Standard 8-node displacement based brick element with tri-linear shape functions.
- Q8A2: Standard displacement based tri-linear brick element with ANS formulation for the transverse shear strain fields E_{13} and E_{23} only.
- Q8A3: Standard displacement based brick element with tri-linear shape functions and ANS formulations for the transverse shear strains E_{13} , E_{23} and in addition for the normal strain E_{33} in thickness direction \mathbf{G}_3 in order to avoid locking effects as they occur in strongly curved structures, discretized by linear elements.
- Q8E1, Q8E3, Q8E4 and Q8E7: The EAS formulation for the thickness strain E_{33} is used with 1, 3, 4 and 7 parameters for the standard displacement based element with tri-linear shape functions according to Klinkel et al. (1997, 1999), Vu-Quoc and Tan (2003), Ramm and Andelfinger (1993) and others.
- Q8A3E1 or Q8A2E1, Q8A3E3 or Q8A2E3, Q8A3E4 or Q8A2E4, Q8A3E7 or Q8A2E7: EAS and ANS formulations are applied for the standard displacement based element with tri-linear shape functions - see interpolation matrix in the appendix.
- Q8S4 and Q8S8: The transverse shear strain field is enhanced with 4 and 8 parameters in the standard displacement element with tri-linear shape functions, the interpolation matrices $\hat{\mathbf{M}}(\xi, \eta, \zeta)$ are defined by linear monomials.
- Q8E1S4 and Q8E1S8: the EAS method is additionally used for the enhancement of the thickness strains in order to locking due to the POISSON effect for the Q8S4 and Q8S8 element in bending deformations.
- Q8S12: The transverse shear strain field is enhanced with 12 parameters in the standard displacement element with tri-linear shape functions. Quadratic polynomials are used in the matrix $\hat{\mathbf{M}}(\xi, \eta, \zeta)$ for the improved transverse strain interpolation to account for the shear deformation theory of second order for thick shells.
- Q8E1S12: Same as Q8S12, but with the EAS method for the linear interpolation of the thickness strain field in order to avoid locking due to the POISSON effect.
- Q4E4 and Q4E4S1: Standard four-node plane stress elements with 4 and 5 EAS-parameters for the improvement of all three strain component of the 2D-model - see Simo and Rifai (1990) and Simo and Armero (1992).

The differences between the results from most elements are caused by the various assumptions of the transverse shear strain interpolation and their treatment in the finite element formulation. Some small deviations among the elements stem from the incorporation of normal strains in thickness direction and are due to the different handling of the thickness strains in the EAS concept.

Figures 4 and 5 show that the elements Q8S12 and Q8E1S12 are the most flexible ones, whereas the standard Q8-brick is the stiffest one. The constant distribution of the transverse normal strains in the tri-linear solid element additionally stiffens the element behaviour in the case of pure bending. The results for the displacements of the EAS-elements Q8S4 or Q8S8 and the ANS-elements Q8A3 are nearly same in both Figures 4 and 5. If the transverse normal strain is interpolated linearly, as it is the case in the elements Q8E1S4, Q8E1S8 and Q8A3E1 or Q8A3E3 and Q8A3E4, the deformation behaviour becomes softer and improves the displacement approximation – see Huettel and Matzenmiller (1999). In order to exclude the influence of the thickness straining from the results for the transverse displacement, the elasticity parameter for POISSON's ratio is set equal to zero in the investigation presented in section 6. The 4-node elements Q4E4 and Q4E4S1 describe the beam in plane stress conditions, which hold exactly, if the width of the beam tends towards zero. Thus, their bending behaviour is softer than the one for the three-dimensional beam models in the general case of a non-vanishing POISSON's ratio.

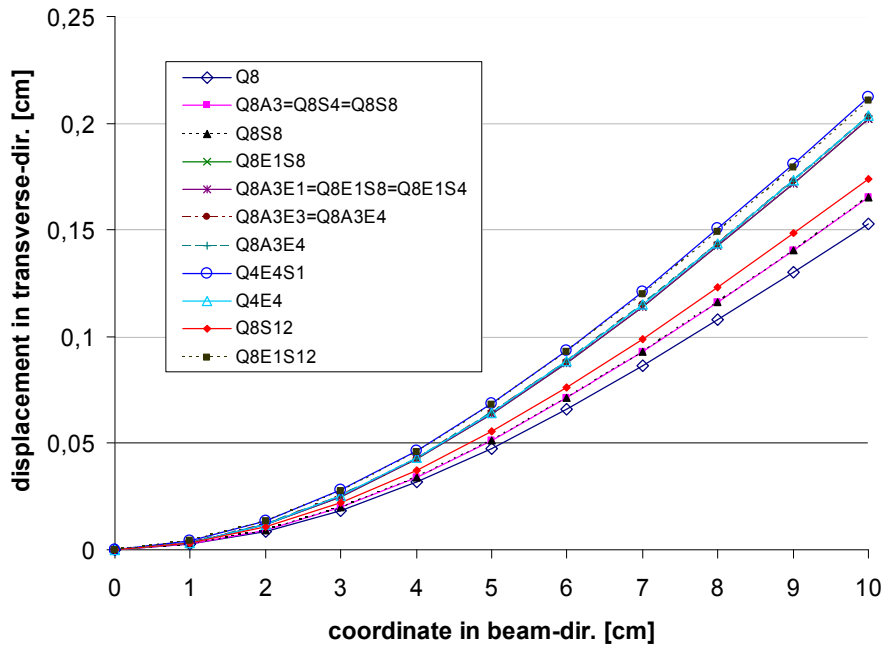


Figure 4. Deflection of beam axis, 1 layer of elements through thickness, isotropic material

The solutions with various finite element formulations are given in Figure 5 for the deflection of the cantilever beam with the transversely isotropic material model. The tendency of the element behaviour is the same as before. The EAS formulation is applied to the normal strain E_{33} in thickness direction for all Q8EXX-elements denoted by E in the appendix EXX. It “softens” especially the elements Q8A3E1, Q8A3E3 and Q8A3E4, where in addition assumed distributions for the natural transverse shear strains E_{13} and E_{23} according to the ANS approach are used to avoid shear locking in the thin shell limit. Although the elements Q8S4, Q8S8 and Q8S12 for the HOSDT, denoted by the characters SXX in the element label do not use the ANS formulation, the numerical results show that they were rather successful and efficient for improving the shear and flexural modes of the deformation.

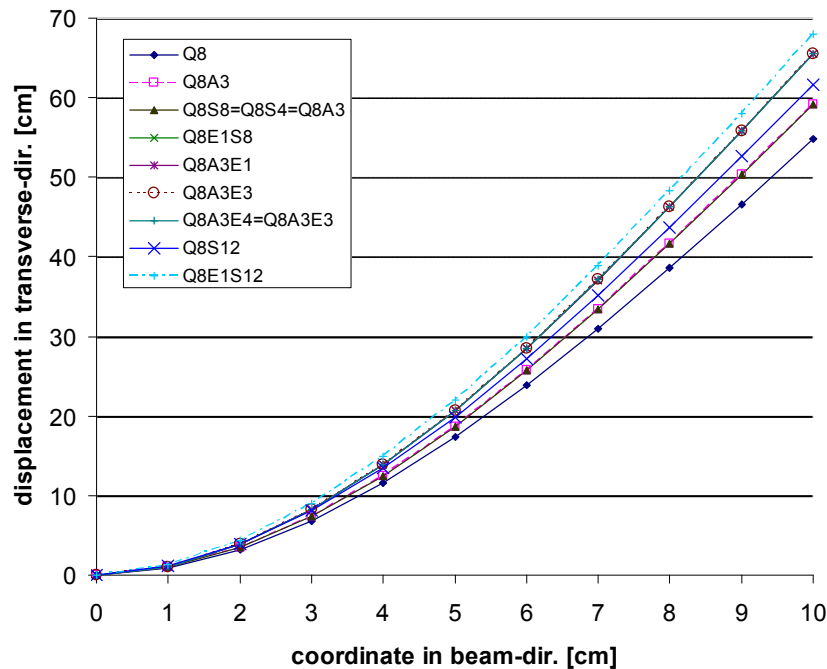


Figure 5. Deflection of beam axis, 1 layer of elements through thickness, transversely isotropic material

The success of especially the quadratic transverse shear approximation on the deflection curve can be quantitatively studied by comparing the results of the isotropic cantilever beam with the mesh of one element

through the thickness to the investigation of a fine discretization with 16 layers of elements in thickness direction, where a sufficiently exact resolution of the transverse shear strain as a step or piecewise linear or parabolic function is obtained. The performance of the 8-node brick element with a parabolic enhancement of the transverse shear strain –see element Q8S12 or Q8E1S12 (with linear normal strains in thickness direction) - in the discretization of the beam with a single layer in Figure 4 may be compared to the analysis of the mesh for 16 tri-linear bricks with constant and linear transverse shear strains as realized in the elements Q8S4 and Q8S8 or Q8A3 in figure 6, where the displacement w in transverse direction along the length of the beam is plotted. It shows again that the elements Q8S12 and Q8E1S12, based on the HOSDT, are the most flexible ones.

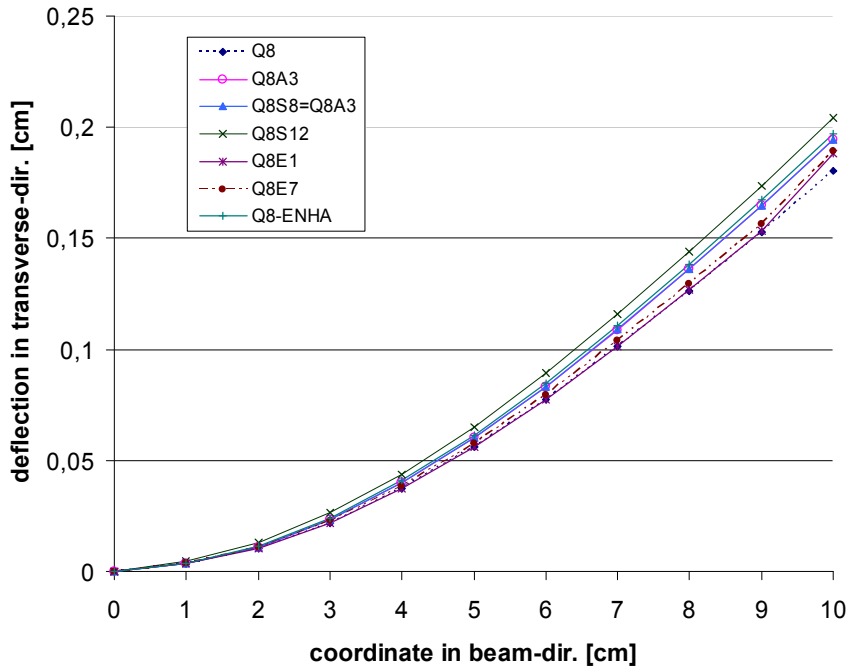


Figure 6. Deflection of beam axis, 16 layers of elements through thickness, isotropic material

In Figure 6 the numerical results are poor for the displacement field of the standard 8-node brick element Q8 as expected and already shown in Figures 4 and 5. The elements Q8E1 and Q8E7 behave as the standard brick Q8 when the Poisson effect does not matter, since no improvement of the transverse shear strain field is carried out. Their displacement field is not significantly better than the one for the standard Q8 element, which improves in the ANS-case, as shown by the element Q8A3. The influence of the transverse normal strain E_{33} on the displacement field is eliminated next, so the approximation error of the transverse shear strain is more isolated.

6 Numerical Results of Cantilever Beam without Transverse Normal Strains

In an additional analysis of the thick beam above, the POISSON'S ratio of the isotropic elasticity model is set to zero ($\nu = 0.0$) in order to suppress the transverse normal strains E_{33} in thickness direction due to the longitudinal bending strain E_{11} . With the same loading at the tip of the cantilever, as given in Chapter 5, the maximum of the deflection is calculated according to engineering mechanics as $w_{\max} = 0.2000 + 0.048 = 0.2048$ cm. The transverse displacement field w along the length of the thick, isotropic beam is plotted for a finite element mesh of one and 16 layers in figures 7 and 8 respectively. The effect of the parabolic shear stress contribution of the Q8S12 element is noticeable when its graph is compared to the one of the Q8S4- and Q8S8-elements, since the parabolic interpolation of the transverse shear strain field softens the element, whereas the linear part in the Q8S4 and Q8S8-brick is hardly provoked in the single layer mesh. Even the small tendency to shear-locking of the standard 8-node brick element Q8 may be seen in this example of a thick beam in both figures. In addition one realizes that the displacements of all ANS-modified elements such as Q8A2, Q8A2S4, Q8A2S8, where only the transverse shear strain fields for E_{13} and E_{23} are manipulated, are about the same as for the Q8S4 and Q8S8 approaches, since the linear interpolation of the transverse shear is not provoked. The calculated displacements of

all elements in the case of normal thickness strains E_{33} identical to zero are very close to the numerical data found for the beam with POISSON's ratio $\nu = 0.4$, as it can be anticipated - compare figures 4 to 7 and 5 to 8.

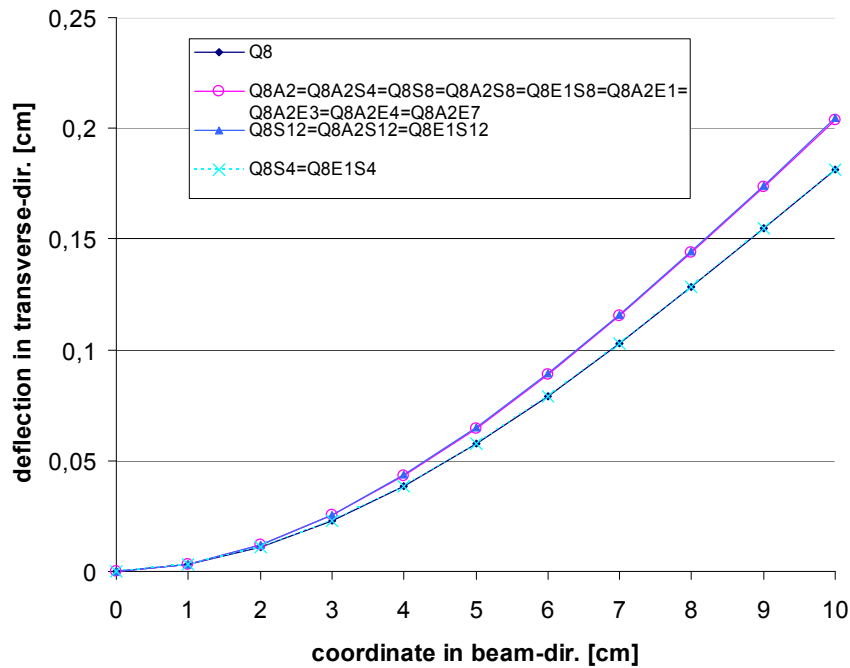


Figure 7. Displacement field over length of thick beam for single layer with POISSON's ratio $\nu = 0.0$

The solution of the mesh with 16 layers of brick elements for the thick, isotropic, clamped beam is depicted in Figure 8 below. All degrees of freedom at the built in edge are suppressed.

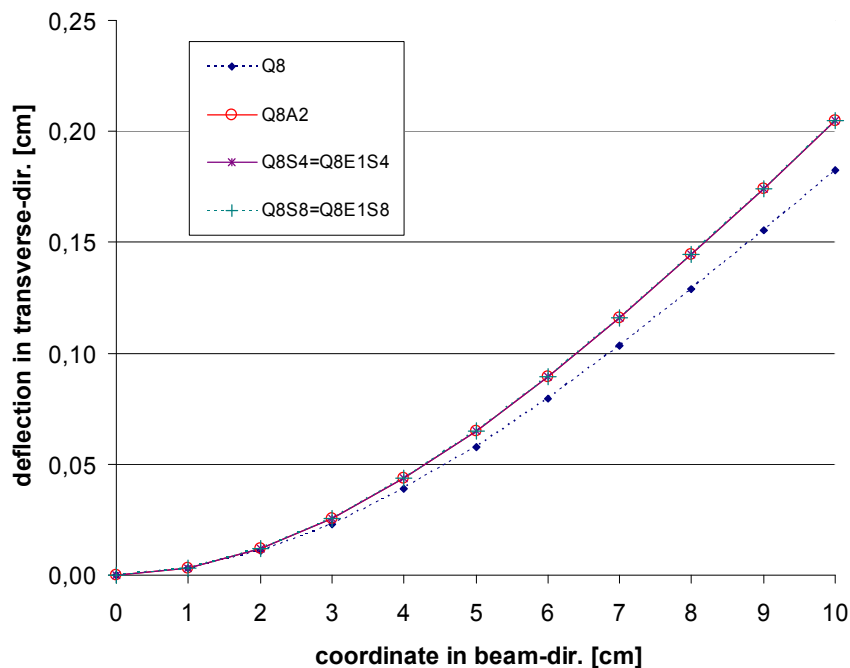


Figure 8. Displacement field of 16 layer mesh for thick beam with POISSON's ratio $\nu = 0.0$

The numerical solutions for the distribution of the transverse shear strain over the thickness in the middle of the beam for the brick elements with different higher order shear interpolations (Q8S4, Q8S8, Q8S12) are compared to the standard 8-node brick element Q8 and to the one with the ANS modification (Q8A2). The FE-solutions are

shown for the single layer mesh in Figure 9. The theoretical solution for the transverse shear strain E_{13} is found from the classical beam theory as $2E_{13_{\max}} = 3P/2Gbh = 6.0 \cdot 10^{-4}$ for its maximum and $2E_{13_{\text{average}}} = P/Gbh = 4.0 \cdot 10^{-4}$ for its average over the cross section with $G = E/2(1 + \nu)$ as the shear modulus of the linear, isotropic elasticity model.

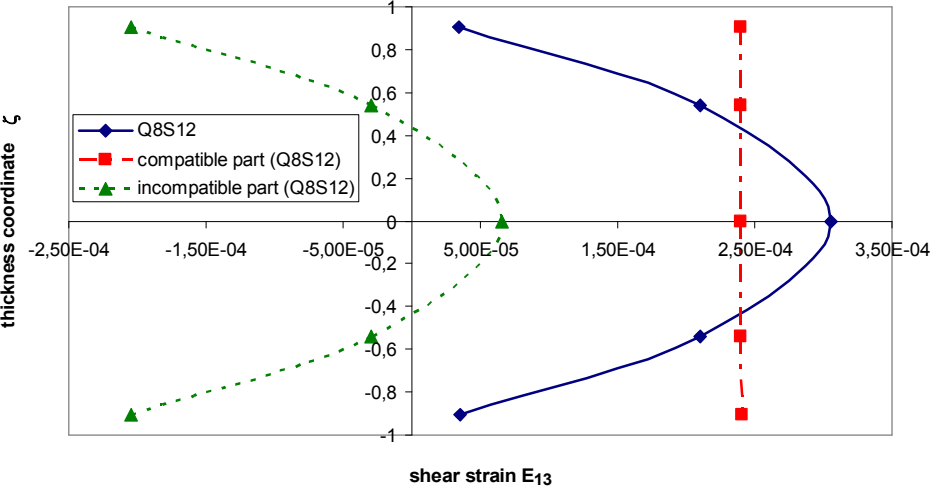


Figure 9. Distribution of total and compatible as well as incompatible part of transverse shear strain E_{13} across thickness for FE- mesh with single layer of elements Q8S12

Figure 10 shows the distribution of the transverse shear stress σ_{13} across the thickness for the thick beam with 1 layer of elements.

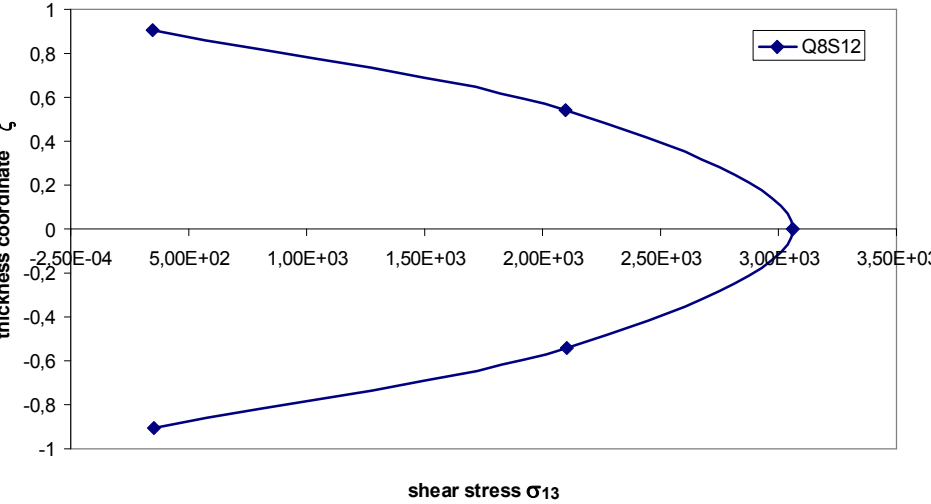


Figure 10. Distribution of transverse shear stress σ_{13} across thickness for FE-mesh with single layer of elements

The solutions of the transverse shear strain are shown for the mesh with 16 layers of elements and various EAS- or ANS-assumptions in Figure 11, where the graph connects the strain results, evaluated at the centre of the elements in the cross section at the middle of the beam.

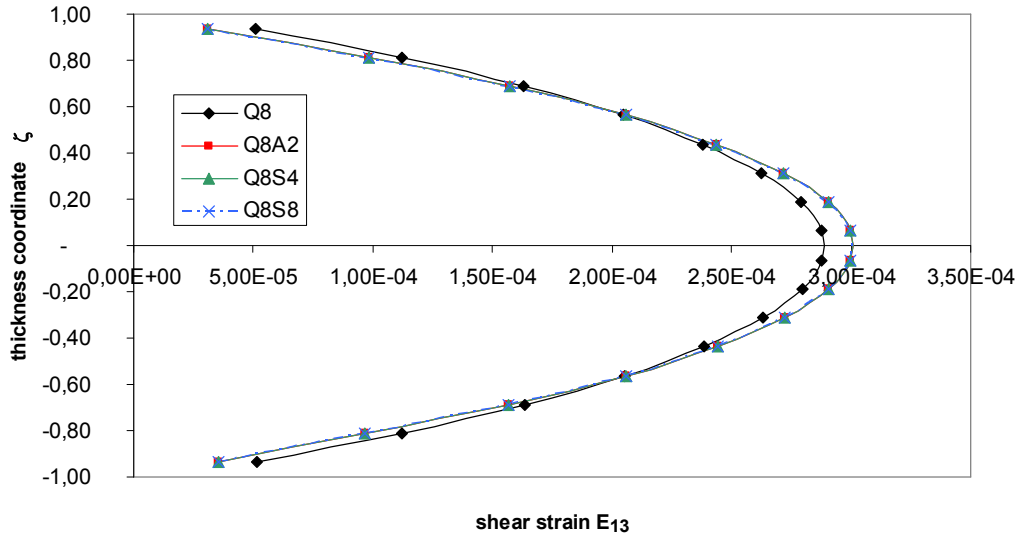


Figure 11. Distribution of transverse shear strain E_{13} across the thickness for FE-mesh with 16 element layers

Thin Beam Example ($L / h = 50$ and 500)

Although the transverse shear deformations are negligibly small in thin beams, a cantilever with a length ($L = 10$ cm) to thickness ratio of $L / h = 500$ and of $L / h = 50$ is analysed in addition with the Q8S12- and Q8S8-element and compared to the standard Q8-model in order to show that the EAS modified elements with the HOSDT are free of shear locking in the thin beam limit. The load P at the tip is reduced each time by a factor of 1000, if the thickness h - taken as 2.0 mm in the thick case, 0.2 mm (thin beam) and 0.02 mm (very thin structure) - decreases by a factor of 10 in order to compensate the reduction of the bending stiffness. The maximum deflection w_{\max} at the tip of the cantilever is listed in table 1 for the element Q8S12 as outlined in eq. (22) and compared to the standard tri-linear solid element Q8 and the EAS element Q8S8 as given in eq. (23).

L / h	w_{\max} for Q8S12	w_{\max} for Q8S8	w_{\max} for Q8
5	0.20422 cm	0.20342	0.18127
50	0.19942 cm	0.19946	0.01482
500	0.19918 cm	0.19918	0.00016

Table 1: Tip deflection of thick (2.0), thin (0.2 cm), and very thin (0.02 cm) cantilever with adapted point load P

As expected the standard hexahedron element Q8 exhibits shear locking, whereas the Q8S12 and Q8S8 model with higher order shear deformations do not, due to the extensions of the first two columns in the matrix \mathbf{M} of eq. (22) and (23).

Sufficiently accurate transverse shear stresses are necessary for the analysis and the design of layered composite beams and shells, where the individual laminae are uni-directionally reinforced with fibres of high tensile strength. The higher order shear deformation theory is applied to the interlaminare fracture analysis of layered beams, which may fail under transverse loading due to their low shear strength.

7 Delamination of Layered Composite Beam – A Short Introduction

One of the most encountered damage mechanisms in layered composite beams is the separation – called delamination – of the laminae from the rest of the plies of the laminate. The cracking at the interface between adjacent layers can cause a significant reduction of the compressive and shear load carrying capacity of a

structure and may initiate structural failure of the beam. In order to prevent delamination, it is necessary to predict accurately its onset and growth. The main work for the investigation of inter-laminar cracking may be divided into the study of the delamination initiation and the analysis of the continuing crack propagation. The simulation of the delamination process in composite structures is quite complex, and requires advanced FE modelling techniques - see Mi et al. (1998), Dávila and Camanho (2001), Iannucci (2006), Morais and Pereira (2007), Reeder (1998) or Fiolka (2008) for example.

The analysis of delamination is usually based on stresses and uses criteria such as the quadratic interaction of the interlaminar stress components in conjunction with a characteristic distance as the critical crack opening displacement. The characteristic distance is an averaging length that is a function of geometry and material properties. Most analyses of delamination growth apply a fracture mechanics approach and evaluate the strain energy release rates G_i for self-similar delamination growth. The strain energy release rates can be computed from the nodal forces and displacements obtained from the solution of a finite element model.

In many structural applications of composites, delamination growth is likely to happen under loads causing mixed-mode fracture. Therefore, a general formulation of the interface elements has to deal with mixed-mode delamination growth. For the cases of loading with pure mode I-, II- or III-deformation the onset of failure can be determined simply by comparing the calculated stress component to their associated strength value of the associated fracture mode. A quadratic failure criterion is used to predict the initiation of delamination in mixed-mode fracture - see figure 12a:

$$\sqrt{\left(\frac{\langle t_1 \rangle}{t_1^{\max}}\right)^2 + \left(\frac{t_2}{t_2^{\max}}\right)^2 + \left(\frac{t_3}{t_3^{\max}}\right)^2} = 1 \quad (25)$$

and a quadratic interaction between the energy release rates for the three modes of fracture is assumed to determine the onset of cracking see figure 12b:

$$\left(\frac{G_I}{G_{IC}}\right)^n + \left(\frac{G_{II}}{G_{IIC}}\right)^n + \left(\frac{G_{III}}{G_{IIIC}}\right)^n = 1, \quad (26)$$

where t_1 , t_2 and t_3 are the components of the stress vector on the interface between the laminae (only tensile and shear stresses), and t_1^{\max} , t_2^{\max} and t_3^{\max} are the nominal strength values for failure in pure tension and pure shear.

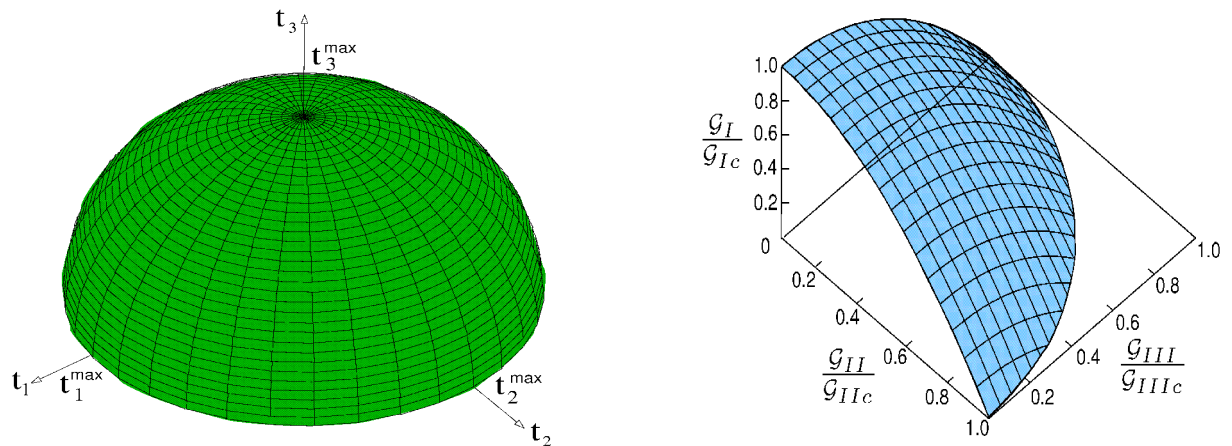


Figure 12. a) Mixed-mode stress criterion of Brewer and Lagace (1998) for mixed-mode failure initiation and b) mixed-mode energy criterion of Dávila and Camanho (2001) for failure mode interaction.

Failure analysis tools must be able to predict the initiation, size and propagation of the delamination process, which is studied at the double cantilever test for single mode fracture and at the mixed-mode bending test for tensile and shear deformation.

Analysis of Double Cantilever Beam (DCB Test)

A popular example for the growth of a delamination is the double cantilever beam test (DCB), which is still under research and further development for the experimental and theoretical investigation of inter-laminar failure of layered composites and adhesively bonded joints. The numerical examples are based on the simulation of delamination growth in a double cantilever beam test, used to determine the toughness of mode I fracture. The specimen is $L=105$ mm long, $b=45$ mm wide, $2h=3.1$ mm thick, and has an initial crack length of $a=20$ mm. YOUNG's modulus of the beam material is $E = 210\,000$ N/mm², POISSON's ratio is $\nu=0.3$, and the energy release rates and critical stresses of the interface element are $G_{IC} = 7.0$ N/mm, $G_{IIC} = 20.0$ N/mm, $t_1^{\max} = 40$ N/mm² and $t_2^{\max} = 44.7$ N/mm². The DCB specimen in the test and in the FE-model are shown in Figure 13.

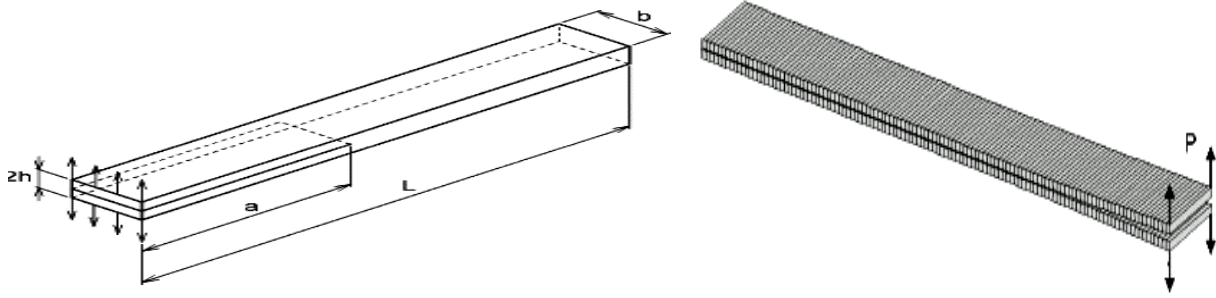


Figure 13. a) Geometry and loading of DCB specimen, b) finite element model of delaminated specimen

The FE-solution of the HOSDT modified elements is shown and compared to the result of the Q8-brick in figure 14 together with the analytical solution for the load-deflection curve in the linear part and for the delamination process as obtained by Mi et al. (1998):

$$P = \frac{3EI}{2a^3} u_{linear} \quad \text{and} \quad u_{delam.} = \frac{2(bG_{IC}EI)^{3/2}}{3EIP^2}. \quad (27)$$

The entire crack opening displacement u at the tip is taken for u_{linear} or $u_{delam.}$ and also used in the plot.

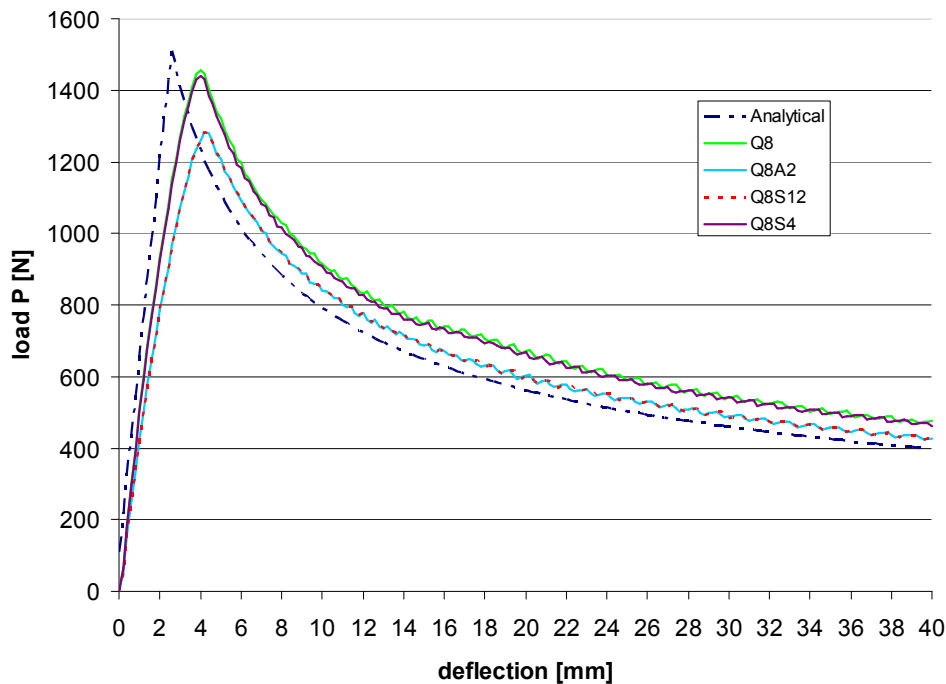


Figure 14. Load-deflection (P-u) diagram of analytical and FE-solutions for DCB test

Analysis of Mixed-Mode Bending Test (MMB Test)

The mixed-mode bending (MMB) test is a simple experiment to measure and identify the delamination toughness in a combination of standard mode I fracture (opening) and mode II cracking (sliding). It comprises as limit cases the double cantilever beam (DCB) test, which is the standard experiment for mode I fracture toughness and the end notched flexure (ENF) test for mode II toughness - see Reeder (1998) and Mi et al. (1998). The enhancement of the MMB test procedure include an improved method for calculating the toughness from the measured test quantities, a more accurate way of setting the mixed-mode ratio in the test, and the inclusion of a new alignment criterion for the improved consistency of the measured values.

Although originally designed to test the static delamination toughness of composites, researchers have extended its use also to fatigue loading and to the toughness testing of adhesives. Because of the number of laboratories using this test, it is important that all relevant test parameters are in accordance with the standardization of the test protocol. Then all simulations and experimental results are directly comparable.

The proportion of mode I and mode II loading in the MMB test is controlled by the setting of the lever loading position c , shown in Figure 15. The MMB test has several advantages with regard to other mixed-mode delamination tests, including the use of a single test specimen configuration and simple load application to test over almost the entire range of mode I to mode II ratios of fracture. As long as the deformations are still small, it has a closed form solution, which is used to calculate the toughness values from measured quantities and a mixed-mode ratio that remains essentially constant during the delamination growth in the entire range of interest.

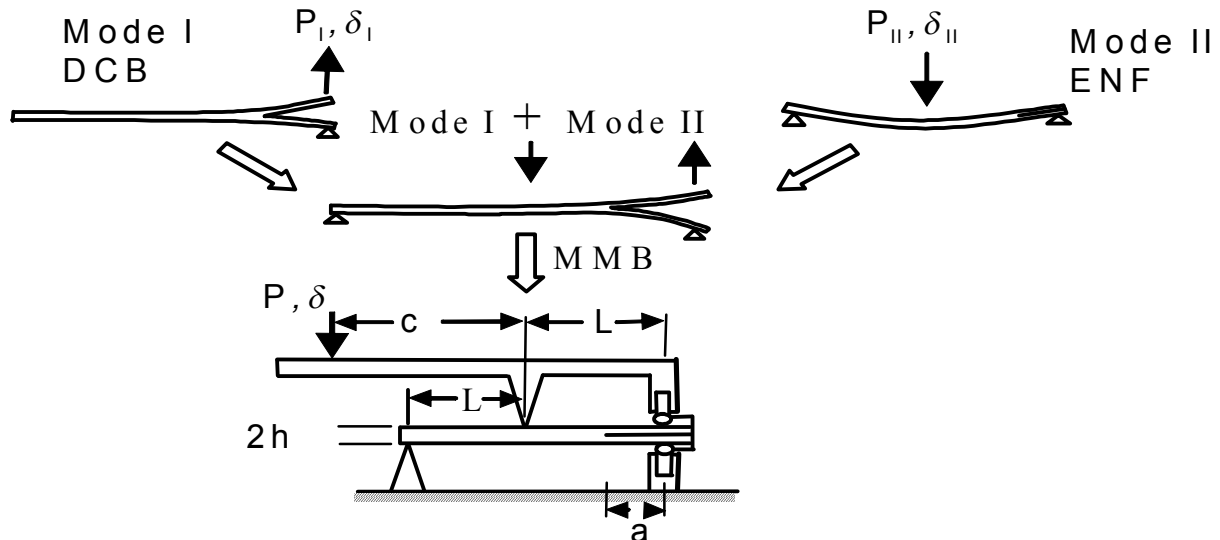


Figure 15. Mixed-mode bending (MMB) test (Reeder, 1998)

The FE-model of the specimen with the super structure for the loading is depicted in Figure 16 a) in its initial configuration and in Figure 16 b) after cracking .

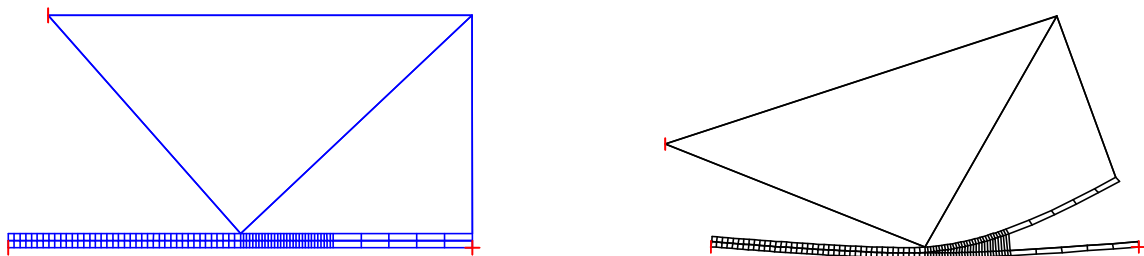


Figure 16. a) FE-model with super structure of undeformed configuration and b) of cracked specimen

The simulation of the standardized MMB test illustrates the successful application of the interface delamination algorithm under mixed-mode loading. In contrast to the linear interaction criterion in Mi et al. (1998), the mixed-

mode interaction parameter n of the power law in the energy criterion above has an assumed value of 2, which results in an ellipsoidal surface for the graphical representation of the criterion. A prescribed motion for displacement control is applied at the end of the lever arm with $c = 41.5$ mm which corresponds to a mixed-mode ratio of $G_I/G_{II} = 1$. For the numerical simulations, the specimen analyzed here has a length ($2L$) of 100 mm, a width (b) of 1 mm and the initial length (a) of the crack is 30 mm. The thickness h of the specimen is 3 mm. The elastic properties of the specimen are given by:

$E_x = 135300$ N/mm², $E_y = E_z = 9000$ N/mm², $G_{xy} = 5200$ N/mm², $\nu_{xy} = \nu_{xz} = 0.24$, $\nu_{yz} = 0.46$ and the energy release rates, the strength values and the elastic stiffness parameters of the interface element are:

$G_{IC} = G_{IIC} = 4.0$ N/mm, $t_1^{\max} = t_2^{\max} = 57$ N/mm² and $K_t = K_n = 10000$ N/mm³ according to Mi et al. (1998) or Dávila and Camanho (2001).

The analytical relation between the load P and the deflection δ prior to crack growth is obviously linear and has been found earlier to be:

$$\delta = \frac{2}{3} \left(\frac{3c-L}{4L} \right) \frac{Pa^3}{EI} \quad (28)$$

The analytical relation for the load/deflection curve during delamination growth has been derived for a $c < L$ as:

$$\delta = \frac{2P}{3EI} \left(\frac{8bEI}{\frac{8P_I^2}{G_{IC}} + \frac{3P_{II}^2}{8G_{IIC}}} \right)^{3/2} \quad (29)$$

Where: $P_I = \frac{(3c-L)}{4L} P$ and $P_{II} = \frac{(c+L)}{L} P$ (30)

The MMB test will turn into pure mode II cracking as in the end-notched flexure experiment (ENF) when the lever loading position c becomes zero. The load-deflection diagrams for the loading point on the lever arm are computed for the ENF ($c = 0.0$) and the MMB ($c = 41.5$ mm) test cases with implicit FE-analysis of the quasi-static displacement equations in contrast to Iannucci (2006) with the standard brick and the modified solid-shell element and plotted in figures 17 and 18:

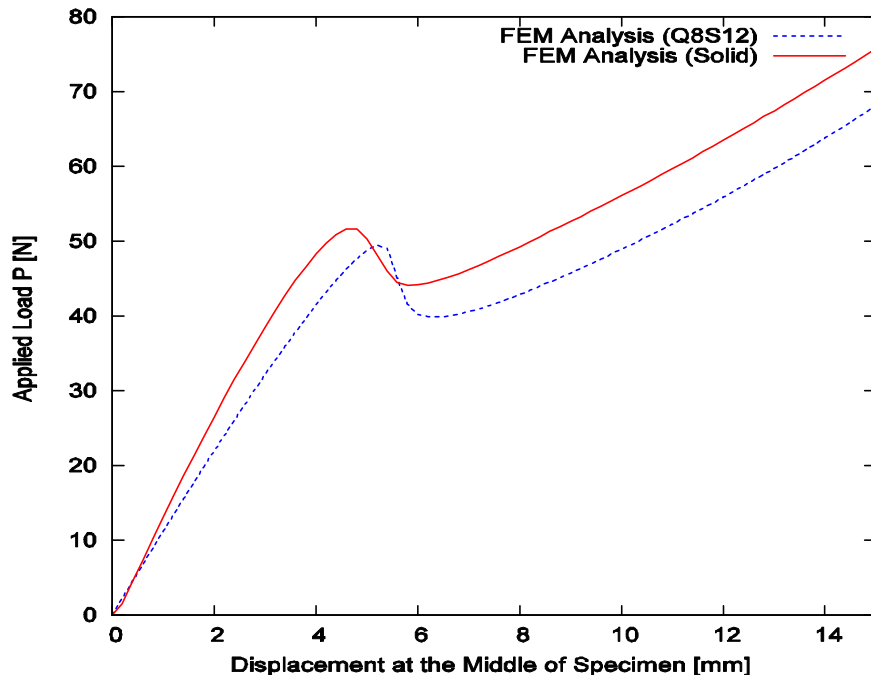


Figure 17. Load-deflection diagram for the ENF test case (mode II)

Figure 18 illustrates the load-displacement diagram of the mixed mode bending case for $c = 41.5$ mm and with the parameters L , b , a , and h as specified above.

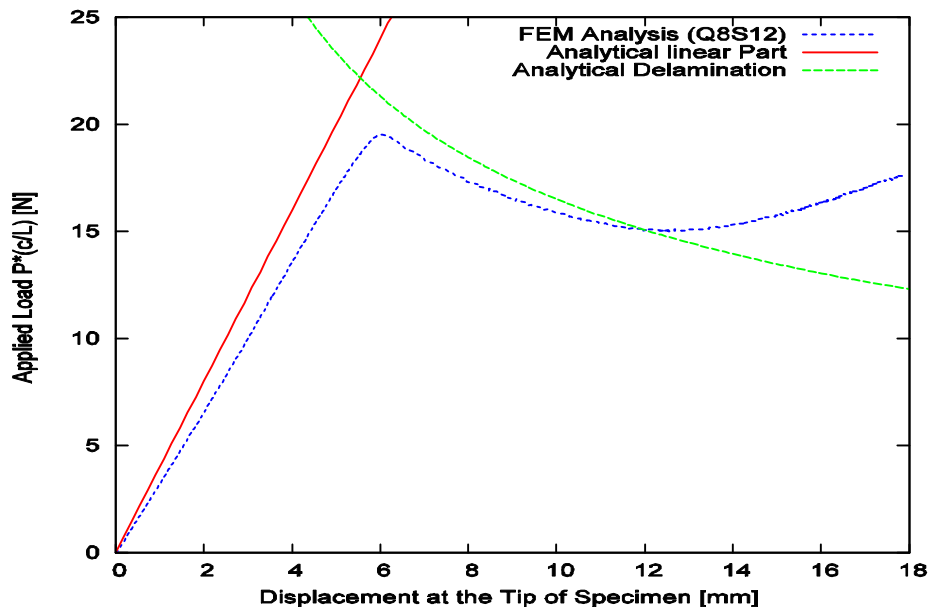


Figure 18. Load-deflection diagram for mixed-mode bending test (MMB) with $c = 41.5$ mm

8 Conclusions and Summary

The paper aims towards the incorporation of the higher order shear deformation theory (HOSDT) into 3D-volume-shell elements by means of the EAS method for the nonlinear analysis of laminated shell structures as demonstrated at the numerical investigation of the double cantilever beam (DCB) and the mixed-mode bending test. New insight is given into the assumption of the higher order transverse shear strain distribution for the successful parabolic shear stress computation with the standard 8-node brick-shell element for shear flexible thin-walled structures.

The numerical results indicate that the higher order transverse shear element shows locking-free bending behaviour. The EAS method for the transverse shear strain discretization may be linked to the high-order shear deformation theory to replace the ANS formulation for the alleviation of shear locking. The combined approach gives the exact solution for the transverse shear stiffness of plate and shells without the need to introduce shear reduction factors such as $5/6$ for the rectangular cross section.

Acknowledgement

The authors gratefully acknowledge helpful support of Dipl.-Ing. Frank Burbulla for testing the solid-shell element with the HOSDT. The first author also thanks the Vietnamese Ministry of Education and Training (MOET) for financial support during his stay at the University of Kassel in Germany.

References

Bathe, K.-J. and E. N. Dvorkin: A formulation of general shell elements – the use of mixed interpolation of tensorial components. *Int. J. Num. Meth. Engng.*, 22, (1986), 697-722.

- Brewer, J. C. and P. A. Lagace: Quadratic stress criterion for initiation of delamination. *J. Compos. Mater.*, 22, (1988), 1141-1155.
- Dávila, C. G. and P. P. Camanho: Decohesion elements using two and three-parameter mixed-mode criteria. American Helicopter Conference, Williamsburg, VA, Oct. 29 - Nov. 1, 2001.
- Fiolka, M.: Theorie und Numerik volumetrischer Schalenelemente zur Delaminationsanalyse von Faserverbundlaminaten, PhD thesis, Institut für Mechanik, Fachbereich Maschinenbau, Universität Kassel, Bericht 2/2008, kassel university press GmbH, (2008).
- Fiolka, M. and A. Matzenmiller: On the resolution of transverse stress in solid-shells with a multi-layer formulation. *Commun. Numer. Meth. Engng.*, 23, (2007), 313-326.
- Fontes Valente, R. A. and P. M. Almeida Areias: Development of shear locking-free shell elements using an enhanced assumed strain formulation. *Int. J. Numer. Meth. Engng.*, 53, (2002), 1721-1750.
- Fontes Valente, R. A., M. P. L. Parente, R. M. Natal Jorge, J. M. A. César de Sá and J. J. Grácio: Enhanced transverse shear strain shell formulation applied to large elasto-plastic deformation problems. *Int. J. Numer. Meth. Engng.*, 62, (2005), 1360-1398.
- Fontes Valente, R. A., R. P. R. Cardoso and J. Whan Yoon: A new approach to reduce membrane and transverse shear locking for one-point quadrature shell elements: linear formulation. *Int. J. Numer. Meth. Engng.*, 66, (2006), 214-249.
- Huettel, C. and A. Matzenmiller: Consistent discretization of thickness strains in thin shells including 3D-material models. *Commun. Numer. Meth. Engng.*, 15, (1999), 283-293.
- Iannucci, L.: Dynamic delamination modelling using interface elements. *Computers and Structures*, 84, (2006), 1029-1048.
- Krätzig, W. B. and D. Jun: Multi-layer multi-director concepts for D-adaptivity in shell theory. Institut für Statik und Dynamik, Ruhr-Universität Bochum, 02/(2002).
- Klinkel, S., F. Gruttmann and W. Wagner: A continuum based 3D-shell element for laminated structures. Institut für Baustatik, Universität Karlsruhe, (1998).
- Klinkel, S., F. Gruttmann and W. Wagner: A robust non-linear solid shell element based on a mixed variational formulation. *Computers and Structures*, 71, (1999), 43-62.
- Klinkel, S. and W. Wagner: A geometrical non-linear brick element based on the EAS method. *Int. J. Num. Meth. Engng.*, 40, (1997), 4529-4545.
- Liu, C. F. and J. N. Reddy: A higher-order shear deformation theory of laminated elastic shells. *Int. J. Eng. Sci.*, 23(3), (1985), 319-330.
- Marotti de Sciarra, F.: Relations between enhanced strain methods and the HR method. *Comput. Methods Appl. Mech. Engrg.*, 191, (2002), 2661-2677.
- Mi, Y., M. A. Crisfield, G. A. O. Davies and H. B. Hellweg: Progressive delamination using interface elements. *J. Compos. Mater.*, 32(14), (1998), 1246-1272.
- Morais de, A. B. and A. B. Pereira: Application of the effective crack method to mode I and mode II interlaminar fracture of carbon/epoxy unidirectional laminates. *Composites Part A: Applied Science and Manufacturing*, 38(3), (2007), 785-794.
- Nguyen, D. Q., R. Schmidt and S. Lenzen: A geometrically nonlinear third-order shear deformation finite plate element incorporating piezoelectric layers. In: Proceedings of the 8th International Conference on Mechatronics Technology (ICMT), Nov. 8-12, 2004, Hanoi, Vietnam.

- Ramm, E. and U. Andelfinger: EAS–elements for two–dimensional, three–dimensional plate and shell structures and their equivalence to HR–elements. *Int. J. Num. Meth. Engng.*, 36, (1993), 1311–1337.
- Rastgaar Aagaah, M., M. Mahinfalah and G. Nakhaie Jazar: Linear static analysis and finite element modeling for laminated composite plates using third order shear theory. *Composite Structures*, 62, (2003), 27-39.
- Reddy, J. N.: *Mechanics of Laminated Composite Plates and Shells: Theory and Analysis*, 2nd edition., CRC Press, Boca Raton, FL (2004).
- Reddy, J. N. and S. J. Lee: Vibration suppression of laminated shell structures investigated using higher order shear deformation theory. *Smart Mater. Struct.*, 13, (2004), 1176-1194.
- Reeder, J. R.: Refinements to the mixed-mode bending test for delamination toughness. NASA Langley Research Center, Hampton, VA, 23681-21199, (1998). <http://citeseer.ist.psu.edu/618357.html>.
- Schweizerhof, K.: 'Solid-shell' elements with linear and quadratic shape functions at large deformations with nearly incompressible materials. Institut für Mechanik, Universität Karlsruhe, (2001).
- Simo, J. C. and F. Armero: Geometrically non-linear enhanced strain mixed methods and the method of incompatible modes. *Int. J. Numer. Meth. Engng.*, 33, (1992), 1413-1449.
- Simo, J. C. and M. S. Rifai: A class of mixed assumed strain methods and the method of incompatible modes. *Int. J. Numer. Meth. Engng.*, 29, (1990), 1595-1638.
- Stander, N., A. Matzenmiller and E. Ramm: An assessment of assumed strain methods in finite rotation shell analysis. *Engineering Computations*, 6(1), (1989), 58-66.
- Taylor, R. L., P. J. Beresford and E. L. Wilson: A non-conforming element for stress analysis. *Int. J. Numer. Meth. Engng.*, 10, (1976), 1211-1219.
- Vu-Quoc, L. and X. G. Tan: Optimal solid shells for non-linear analyses of multilayer composites. *Comput. Methods Appl. Mech. Engng.*, 192, (2003), 975–1016.
- Wilson, E. L., R. L. Taylor, W. P. Doherty and J. Ghaboussi: Incompatible displacement models. In: S. J. Fenves et al. (eds.), *Numerical and Computer Models in Structural Mechanics*, Academic Press, New York, (1973).

Appendix

The interpolation matrices $\mathbf{M}(\xi, \eta, \zeta)$ for the enhanced strain part of the EAS modified elements are given here together with the ANS notation for solid-shell elements as outlined in Klinkel et al. (1999):

- a. Q8: Standard displacement element with tri–linear shape functions.
- b. Q8A3: Standard displacement element with tri–linear shape functions, using ANS formulations for E_{13} , E_{23} and E_{33} ; Q8A2: ANS formulation is used for E13 and E23 only (without any EAS modifications).
- c. Q8A3E1 element (or Q8A2E1): same as Q8 but in addition with EAS and ANS formulations; element Q8E1 uses only a linear monomial in the thickness coordinate for the enhanced transverse normal strain in order to account for the POISSON effect in the direction of the element’s normal in the case of bending:

$$\mathbf{M}(\xi, \eta, \zeta) = \begin{bmatrix} 0 \\ 0 \\ \zeta \\ 0 \\ 0 \\ 0 \end{bmatrix}$$

- d. Q8A3E3 element (or Q8A2E3) same as Q8 but in addition with EAS and ANS formulations; element Q8E3 uses only an incomplete linear interpolation for the enhanced transverse normal strain field:

$$\mathbf{M}(\xi, \eta, \zeta) = \begin{bmatrix} 0 & 0 & 0 \\ 0 & 0 & 0 \\ \zeta & \zeta\xi & \zeta\eta \\ 0 & 0 & 0 \\ 0 & 0 & 0 \\ 0 & 0 & 0 \end{bmatrix}$$

- e. Q8A3E4 element (or Q8A2E4) same as Q8 but in addition with EAS and ANS formulations; element Q8E4 uses only enhanced transverse normal strains with a complete linear interpolation:

$$\mathbf{M}(\xi, \eta, \zeta) = \begin{bmatrix} 0 & 0 & 0 & 0 \\ 0 & 0 & 0 & 0 \\ \zeta & \zeta\xi & \zeta\eta & \zeta\xi\eta \\ 0 & 0 & 0 & 0 \\ 0 & 0 & 0 & 0 \\ 0 & 0 & 0 & 0 \end{bmatrix}$$

- f. Q4E4 and Q4E4S1 standard four-node plane elements (for the plane stress problem):

$$\mathbf{M}(\xi, \eta, \zeta) = \begin{bmatrix} \xi & 0 & 0 & 0 \\ 0 & \zeta & 0 & 0 \\ 0 & 0 & \xi & \zeta \end{bmatrix} \quad \text{with } 2 \times 2 \text{ GAUSS integration points and}$$

$$\mathbf{M}(\xi, \eta, \zeta) = \begin{bmatrix} \xi & 0 & 0 & 0 & 0 \\ 0 & \zeta & 0 & 0 & 0 \\ 0 & 0 & \xi & \zeta & \zeta^2 \end{bmatrix} \quad \text{with } 2 \times 3 \text{ GAUSS integration points}$$

- g. Q8E1S4 element same as Q8S4 but in addition with enhanced transverse normal strain field by means of a linear monomial - see also eq. (23a):

$$\mathbf{M}(\xi, \eta, \zeta) = \begin{bmatrix} 0 & 0 & 0 & 0 & 0 \\ 0 & 0 & 0 & 0 & 0 \\ \zeta & 0 & 0 & 0 & 0 \\ 0 & 0 & 0 & 0 & 0 \\ 0 & \xi & 0 & \xi\eta & 0 \\ 0 & 0 & \eta & 0 & \xi\eta \end{bmatrix},$$

in order to avoid POISSON-locking for the Q8S4 element.

- h. Q8E1S8 element same as Q8S8 but in addition with enhanced transverse normal strain field by means of linear monomials - see also eq. (23b):

$$\mathbf{M}(\xi, \eta, \zeta) = \begin{bmatrix} 0 & 0 & 0 & 0 & 0 & 0 & 0 & 0 & 0 \\ 0 & 0 & 0 & 0 & 0 & 0 & 0 & 0 & 0 \\ \zeta & 0 & 0 & 0 & 0 & 0 & 0 & 0 & 0 \\ 0 & 0 & 0 & 0 & 0 & 0 & 0 & 0 & 0 \\ 0 & \xi & \zeta & 0 & 0 & \xi\eta & \xi\zeta & 0 & 0 \\ 0 & 0 & 0 & \eta & \zeta & 0 & 0 & \xi\eta & \eta\zeta \end{bmatrix},$$

in order to avoid Poisson- locking for the Q8S8 element.

- i. Q8E1S12 element with enhanced transverse shear and normal strain fields in order to avoid locking due to the POISSON effect in the Q8S12 element - see eq. (22) for the high-order SDT:

$$\mathbf{M}(\xi, \eta, \zeta) = \begin{bmatrix} 0 & 0 & 0 & 0 & 0 & 0 & 0 & 0 & 0 & 0 & 0 & 0 & 0 & 0 \\ 0 & 0 & 0 & 0 & 0 & 0 & 0 & 0 & 0 & 0 & 0 & 0 & 0 & 0 \\ \zeta & 0 & 0 & 0 & 0 & 0 & 0 & 0 & 0 & 0 & 0 & 0 & 0 & 0 \\ 0 & 0 & 0 & 0 & 0 & 0 & 0 & 0 & 0 & 0 & 0 & 0 & 0 & 0 \\ 0 & \xi & 0 & \xi\eta & 0 & \frac{1}{5} - \zeta^2 & 0 & \xi\left(\frac{1}{5} - \zeta^2\right) & \eta\left(\frac{1}{5} - \zeta^2\right) & 0 & 0 & \xi\eta\left(\frac{1}{5} - \zeta^2\right) & 0 & 0 \\ 0 & 0 & \eta & 0 & \xi\eta & 0 & \frac{1}{5} - \zeta^2 & 0 & 0 & \xi\left(\frac{1}{5} - \zeta^2\right) & \eta\left(\frac{1}{5} - \zeta^2\right) & 0 & \xi\eta\left(\frac{1}{5} - \zeta^2\right) & 0 \end{bmatrix}$$

- j. Q8A3E7 element (or Q8A2E7): EAS (and additionally ANS) formulations are used – see below; Q8E7: EAS modifications are applied without ANS formulations according to Vu-Quoc and Tan (2003) – see below:

$$\mathbf{M}(\xi, \eta, \zeta) = \begin{bmatrix} \xi & 0 & 0 & 0 & 0 & 0 & 0 \\ 0 & \eta & 0 & 0 & 0 & 0 & 0 \\ 0 & 0 & \zeta & \zeta\xi & \zeta\eta & 0 & 0 \\ 0 & 0 & 0 & 0 & 0 & \xi & \eta \\ 0 & 0 & 0 & 0 & 0 & 0 & 0 \\ 0 & 0 & 0 & 0 & 0 & 0 & 0 \end{bmatrix}$$

Addresses:

Nguyen Dang Quy, Institute of Applied Mechanics, Vietnamese Academy of Science and Technology, 291 Dien Bien Phu, Ho Chi Minh City, Vietnam, Visiting scholar at the Institute of Mechanics, Department of Mechanical Engineering, University of Kassel, Moenchebergstr. 7, D-34109 Kassel.

Prof. Dr.-Ing. Anton Matzenmiller, Institute of Mechanics, Department of Mechanical Engineering, University of Kassel, Moenchebergstr. 7, D-34109 Kassel.

email: nguyendam2003@yahoo.ie; amat@ifm.maschinenbau.uni-kassel.de